Classical and Quantum Gravity

PAPER

The facilities and performance of TianQin laser ranging station

To cite this article: Caishi Zhang *et al* 2022 *Class. Quantum Grav.* **39** 125005

IOP Publishing Classical and Quantum Gravity

Class. Quantum Grav. **39** (2022) 125005 (20pp) https://doi.org/10.1088/1361-6382/ac6d3e

The facilities and performance of TianQin laser ranging station

Caishi Zhang[1], Tianquan Gao[1,10], Yuyan Cao[2], Zhongwei Fan[3], Honglin Fu[4], De-Feng Gu[1], Xida Han[1], Yutao Huang[3], Lin Kang[5], Ke Li[6], Ming Li[1,*], Rongwang Li[4], Yu-Qiang Li[4], Zhulian Li[4], Zun-Biao Li[1], Jun-Xiang Lian[1], Junchi Liu[2], Qi Liu[1], Sheng-Qian Liu[1], Yuan Liu[1], Jianwei Mei[1], Xiaoyu Pi[4], Cheng-Gang Shao[7], Ji Sun[8], Yu-Jie Tan[7], Yuhua Tang[9], Liang-Cheng Tu[1,*], Panpan Wang[7], Saijin Wang[6], Peiheng Wu[5], Qinglin Wu[2], Liang Xiong[8], Yao-Heng Xiong[4], Chao Xue[1], Yong Yan[1], Shan-Qing Yang[1], Hsien-Chi Yeh[1,*], Dongsheng Zhai[4], Haitao Zhang[4], Hongbo Zhang[3], Labao Zhang[5], Lihua Zhang[8], Hong-Chao Zhao[1], Guo-Dong Zhou[9] and Jun Luo[1,*]

[1] MOE Key Laboratory of TianQin Mission, TianQin Research Center for Gravitational Physics & School of Physics and Astronomy, Frontiers Science Center for TianQin, Gravitational Wave Research Center of CNSA, Sun Yat-sen University (Zhuhai Campus), Zhuhai 519082, People's Republic of China

[2] Changchun Institute of Optics, Fine Mechanics and Physics, Chinese Academy of Science, Changchun, 130033, People's Republic of China

[3] Academy of Opto-Electronics, Chinese Academy of Science, Beijing, 100094, People's Republic of China

[4] Yunnan Observatories, Chinese Academy of Science, Kunming, 650216, People's Republic of China

[5] School of Electronic Science and Engineering, Nanjing University, Nanjing, 210093, People's Republic of China

[6] Beijing Aerospace Control Center, Beijing, 100094, People's Republic of China

[7] Centre for Gravitational Experiments, School of Physics, MOE Key Laboratory of Fundamental Physical Quantities Measurement & Hubei Key Laboratory of Gravitation and Quantum Physics, PGMF, Huazhong University of Science and Technology, Wuhan 430074, People's Republic of China

[8] DFH Satellite Co., Ltd., China Academy of Space Technology, Beijing 100094, People's Republic of China

[9] Lunar Exploration and Space Program Center, Beijing, 100048, People's Republic of China

[*] Authors to whom any correspondence should be addressed.
[10] Co-first author.

E-mail: liming73@mail.sysu.edu.cn, tuliangch@mail.sysu.edu.cn, yexianji@mail.sysu.edu.cn and junluo@sysu.edu.cn

Received 24 February 2022, revised 4 May 2022
Accepted for publication 5 May 2022
Published 25 May 2022

Abstract

The TianQin Project is aiming at gravitational wave (GW) detection in space. TianQin GW observatory comprises three satellites orbiting on 1×10^5 km Earth orbits to form an equilateral-triangle constellation. In order to minimize the variations in arm lengths and breathing angles, the satellites must be launched and adjusted precisely into an optimized orbit. Therefore, satellite laser ranging must be used to enhance the precision of satellite orbit determination. To develop the capability of satellite laser ranging for TianQin's orbit, the TianQin Laser Ranging Station has been designed and constructed to perform high-precision laser ranging for TianQin satellites and lunar laser ranging as well. Applying a 1064 nm Nd: YAG laser with 100 Hz repetition frequency, 80 pico-second pulse duration, and 2×2 array of superconducting nanowire single-photon detectors, we have obtained the laser echo signals from the five lunar retro-reflector arrays, and the measurement data have been packaged into 234 normal points (NPs), including a few data measured during the full-moon lunar phase. Each NP is calculated from continuous measurement for about ten minutes and the statistical error of the NPs is about 7 mm (1σ).

Keywords: lunar laser ranging, satellite laser ranging, precision satellite orbit determination, gravitational waves detection

(Some figures may appear in colour only in the online journal)

1. Introduction

1.1. Requirements of satellite's orbit determination for TianQin

Proposed in 2014, the TianQin Project aims to launch a space-based GW observatory to detect GW in the frequency band of 10^{-4} Hz–1 Hz. The three satellites will be launched to high Earth orbits of 1×10^5 km around 2035, and the constellation plane is nearly vertical to the ecliptic and facing a white dwarf binary star system, J0806.3 + 1527 [1, 2].

The requirements for the arm-length variation, the relative line-of-sight velocity and the breathing angle of the TianQin constellation during the measurement period are stringent. As the constellation stability is very sensitive to the initial position and initial velocity of the satellites' orbits, it is of great importance for achieving a high-precision satellite orbit determination. Preliminary analysis showed that the accuracy of initial position and initial velocity of TianQin satellites must be 5 m and 2 mm s^{-1}, respectively [3].

Satellite laser ranging (SLR) is the space geodetic technique with the highest precision of range measurement [4]. It is commonly used either to calibrate the accuracy or to compensate the error of satellite's orbit determination [5], to determine the station coordinates [6, 7], Earth orientation parameters (EOP) [8], and tidal parameters [9, 10]. Studying the Earth's gravity field, the ocean tide models [11, 12], and the elasticity [9, 13]. However, due to the limitation of observation (weather) conditions, it generally needs to work together with the orbital dynamic models with long measurement arcs for dynamic orbit determination. There is about 15% coverage of long-arc-length observation data which are provided by the International Laser Ranging Service (ILRS), especially for medium-altitude and high-altitude Earth orbit navigation satellites [14].

We have done the simulation analysis on TianQin satellite's orbit determination, assuming that the ranging data were obtained from seven worldwide laser ranging stations, with a minimum observation elevation of 30°, with an observation rate of 15% and with a statistical error of about 1 cm. The simulation results show that the positioning accuracy in three dimensions can reach 1.69 m, and the velocity accuracy is about 0.12 mm s^{-1}. The detailed discussion will be reported in another paper.

So far, most of the satellites equipped with retro-reflectors are operating below the geosynchronous orbit. To ensure a sufficient budget of laser ranging capability for TianQin satellites, the lunar retro-reflectors are ideal targets for testing and evaluating the performance of a new laser ranging station built inside the Zhuhai campus of Sun Yat-sen University.

1.2. Current status of lunar laser ranging (LLR)

Since the first manned Moon landing mission, Apollo 11, there had been five retro-reflector arrays deployed on the Moon, enabling the highly accurate range measurements between the ground station and the lunar retro-reflectors by means of laser ranging [15]. The design of retro-reflector arrays is based on a corner-cube structure, such that the laser beam can be reflected back along the direction parallelly to the incident direction. The Apollo astronauts deployed three arrays with 100 and 300 corner-cube retro-reflectors of 38 mm diameter, mounted in aluminum panels. The soviet-French Lunokhod arrays consist of 14 triangular retro-reflectors of 106 mm side-length, arranged in a two-row hexagonal packing. Accumulated LLR measurement data shows these five retro-reflector arrays functioning well, including Lunokhod 1 which was precisely located by Apache Point Observatory until 2010 [16].

Because of the long distance between Earth and the Moon which accounts for the serious power loss of echo signals in laser ranging, only a few observatories are capable of doing LLR. The Lick Observatory started the LLR experiment, and then the McDonald Observatory with a 2.7 m telescope and its upgraded McDonald Laser Ranging Station with a 0.76 m telescope proceeded. A massive data is contributed by Grasse laser station located in France. Other renowned stations include Haleakala (USA), Apache Point Observatory Lunar Laser Ranging Operation (APOLLO, USA) and Matera (Italy). The Wettzell station (Germany) has contributed some NPs in recent years, and the Yunnan station (China) succeeded in LLR in 2018 [17]. Currently, only APOLLO, Grasse, Matera and Wettzell stations are carrying out regular LLR observation. Till October 2021, there are 29743 NPs are provided on the ILRS. The contribution and the duration of LLR data are shown in figure 1. (The LLR data is from ILRS[11] and POLAC[12]).

The basic principle of LLR is currently based on the measurement of the round-trip time of flight (TOF) of a laser pulse travelling between the Earth's station and the lunar retro-reflectors. With the speed of light in vacuum c, the range can be obtained by using equation (1)

$$L = c \cdot \Delta t/2, \tag{1}$$

where Δt is the round-trip travelling time of the laser pulse.

[11] https://cddis.nasa.gov/archive/slr/data/npt_crd/.
[12] http://polac.obspm.fr/llrdata.html.

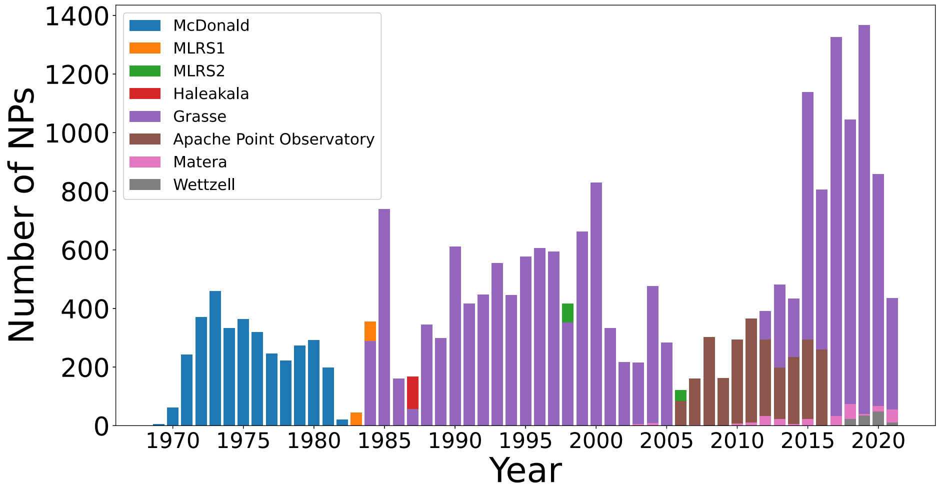

Figure 1. Number of NPs acquired per year of LLR stations.

The Earth–Moon system is a natural laboratory for testing general relativity. Studying the dynamics of the Earth–Moon system is of great importance for testing gravitational theories and exploring the internal structure of the Moon. The best results of the test of strong equivalence principle [18–20], the test of Newtonian inverse square law [21], the determination of time-varying gravitational constant [22, 23] have been obtained by means of LLR [24, 25].

The precision of LLR has been improved from decimeter-level to a few millimeters over decades. So far, the precision of LLR is limited by the performance of the laser ranging system, the array structure of lunar retro-reflector [26] and their degraded reflection efficiency [27] and finally, by the tilt of the retro-reflector array due to Lunar libration, which increases the random error of the TOF of the laser beam reflected from different array elements. In order to solve the problem, the design of single large-aperture corner-cube retro-reflectors for next-generation LLR was proposed [28, 29]. Researchers from Sun Yat-sen University and Huazhong University of Science and Technology have manufactured a 170 mm hollow corner-cube retro-reflector, which has been carried by the 'QueQiao' relay satellite on 21 May 2018 to test its performance in space [30, 31].

The construction of the TianQin laser ranging station (ab. TianQin station in the following) had completed in January 2019. It is located at the Zhuhai campus of Sun Yat-sen University at an altitude of about 400 m. The first successful LLR experiment was carried out on 8 June 2019, and the five lunar retro-reflector arrays were successfully detected on 7 November 2019. The observations from June 2019 to November 2020 have been packaged into 234 NPs, each NP is calculated from ten-minute continuous measurement data. In the following sections, the overview of the ranging system of TianQin Station is briefly introduced. In section 3, the random errors of laser ranging are evaluated, and typical LLR results are presented. Finally, we discuss the performance of laser ranging improved by using an infrared laser and superconducting single-photon detector array.

2. Overview of ranging system

The instruments and optical path of the TianQin laser ranging system are shown in figure 2. The system consists of a 1.2 m telescope and Nd: YAG laser with single pulse energy of 300 mJ and

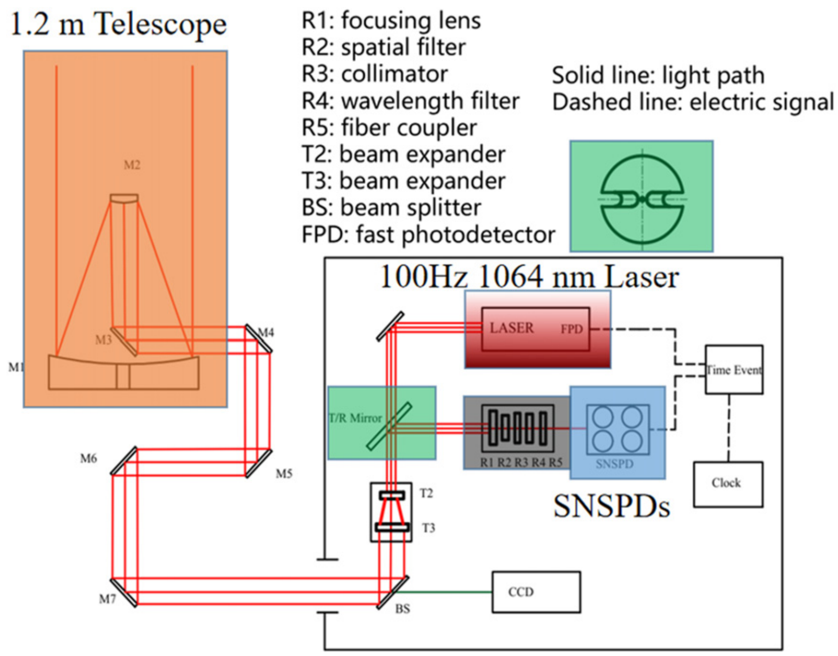

Figure 2. Optical path and facilities of TianQin Station.

Table 1. Main parameters of TianQin Station.

Parameter	Value	Comment
λ	1064 nm	Laser wavelength
E_t	0.3 J	Laser pulse energy
f_{pulse}	100 Hz	Laser pulse repetition rate
D	1.2 m	Aperture of the telescope
θ_{laser}	$2''$	Divergence angle of laser
θ_{track}	$2''$	Tracking error of telescope
η_t	0.6	Transmitting efficiency of optical system
η_r	0.2	Receiving efficiency of optical system

a pulse width of 80 ps. The repetition frequency of this pulsed laser is 100 Hz, operating at a wavelength of 1064 nm. To ensure a better detection efficiency, a 2×2 superconductor nanowire single-photon detector array is used. The technical specifications of this laser ranging system are shown in table 1. Compared with other LLR systems, the major features of this system are the use of a 1064 nm laser with a repetition frequency of 100 Hz and a new type of detector array for LLR. Principally speaking, a higher pulse repetition rate makes a lower random error and a larger echo photon number per unit time.

A common light path system has been adopted at TianQin Station. The optical train has a transmit path and a receive path that share the telescope as shown in figure 2. A rotation mirror (as shown in the figure 2 (green)) separates the laser transmit path and the receive path similar to Apache Point Observatory set-up [32]. The rotation repetition of the T/R optic is well controlled to 50 Hz, and two transmit holes of the T/R optic are designed to match the

Table 2. Expected gain in the infrared compared to the green link.

Expected gain in IR compared to green link		
Elevation angle	20°	40°
Laser	3	3
Divergence	1.3″	1.3″
Atmospheric transmission	1.9^2	1.32^2
Velocity aberration	1.28	1.28
Total gain IR/green	18.02	8.70

laser repetition frequency (100 Hz). The receive path is split into two beams through a beam splitter, one of which is sent toward a charge-coupled device camera that aids acquisition and alignment, another to the receiving detector. Temporal filtering (range gate), spatial filtering (a pinhole), and spectral filtering (narrow pass-band filter) are used to suppress the background noise from the lunar surface, atmospheric back-scattering, and optical lens back-scattering, as shown in figure 2 (gray).

2.1. The advantages of 1064 nm

Due to the excellent detection performance of the detector in the visible spectral band, most LLR observatories adopt a 532 nm laser as the light source which is generated from Nd: YAG laser and second harmonic generation (SHG). They have suffered signal acquiring during new and full Moon phases with a green laser. First applying the 1064 nm infrared laser at Grasse laser ranging station allows LLR measurements during those periods [33]. Wettzell laser ranging station also has acquired LLR signal in infrared. Beyond the detection efficiency of detectors at two different wavelengths, there are some advantages to using near-infrared compared with green laser in the following aspects:

(a) Atmospheric transmission. The atmospheric attenuation is a function of wavelength, local atmosphere seeing, the altitude of a station, etc. The atmospheric transmittance at 1064 nm is better than that at 532 nm in different elevations [4].
(b) The number of photons. The number of photons at 1064 nm is twice that of 532 nm with the same energy. The 532 nm laser is acquired through SHG from the 1064 nm laser, and the efficiency of SHG is about 50%. The ratio of the number of transmitting photons at 1064 nm to that at 532 nm with the same energy will be greater than 2.
(c) Beam divergence propagating through the atmosphere. Affected by the external atmospheric turbulence, the diffraction limit is not determined by the aperture of the telescope, but by the Fried parameter r_0 [34], which is related to the atmospheric parameter (atmospheric seeing) of the station and laser. r_0 increases with the increasing of wavelength, corresponding to a smaller radius of the Gaussian beam propagating in the atmosphere at 1064 nm.
(d) Effect of velocity aberration. Due to the relative motion of the Moon and the rotation of the Earth, the energy received by the telescope is not in the center of the Airy Disk [35]. The distribution of the far-field diffraction pattern is related to the laser wavelength, corresponding to a disk with more concentrated energy at 1064 nm.

Given the above factors, the analysis results in the paper [33] are used, as shown in table 2. The results show that there are obvious advantages in the LLR experiment at 1064 nm.

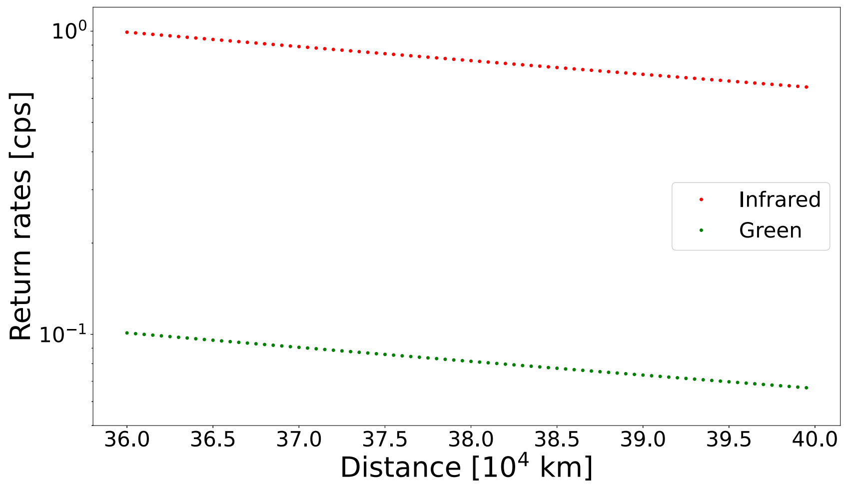

Figure 3. Comparison of theoretic return rates between 1064 nm and 532 nm varies with distance.

2.2. Theoretical calculation of the number of photons

For a space target equipped with the retro-reflector, the number of theoretical return photons recorded by detectors is as follows [4]:

$$n_0 = \frac{\lambda}{hc} \cdot E_{\mathrm{t}} \cdot T^2 \cdot \eta_{\mathrm{t}} \cdot \eta_{\mathrm{r}} \cdot \frac{4 \cdot D^2 \cdot \rho \cdot \sigma}{\pi \theta_{\mathrm{ccr}}^2 \cdot \theta_{\mathrm{t}}^2 \cdot R^4} \cdot \alpha \cdot f_{\mathrm{pulse}}, \tag{2}$$

where λ is the laser wavelength, f_{pulse} is the frequency of the laser, h is Planck's constant, E_{t} is the energy of a single pulse, T is the atmospheric transmittance, η_{t} and η_{r} are the efficiency of the transmitting optics and the receiving optics, respectively, σ is the retro-reflector optical cross-section, ρ is the reflectivity of the target, D is the effective receiving aperture of the telescope, θ_{ccr} is the divergence angle of the corner cube reflector, α is attenuation coefficient.

The theoretical return counts per second (cps) of Apollo 15 is simulated when the elevation angle of observation is 40° with the parameters shown in tables 1 and 2, and the results are shown in figure 3. Red and green dots represent the theoretical calculation return rates at 1064 nm and 532 nm, respectively. The return rates decrease with the increasing distances. More importantly, more effective echo photon counts will be acquired at 1064 nm compared with 532 nm in the same experimental conditions, which shows the performance at 1064 nm is significantly superior to that at 532 nm.

2.3. Detection probability analysis of four-pixel SNSPD array

Apart from the theoretical return rates, the detection probability is another important parameter to describe the performance of a laser ranging system. Due to the excellent quantum efficiency at single-photon level detection, avalanche photon diode (APD) is a routine detector applied for SLR and LLR. SNSPD is widely used for quantum key distribution and quantum communication [36] with its excellent characteristics such as a large detection area (diameter = 60 μm), low time jitter (<80 ps), broadband response (0.4–2 μm), high quantum efficiency (>90%), extremely low dark count rate (DCR) (100 Hz), and high repetition rate (20 MHz). Since the subcentimeter depth profiling was demonstrated at a distance of 330 m on the ground [37].

The SNSPD was also applied for space target detection, e.g. SLR [38] and space debris laser ranging [39], which have proven the capability for space target laser ranging.

Here, we will analyze the detection probability of APD and SNSPD, as well as how the number of pixels of the two kinds of detectors will influence the detection probability. Assuming that the effective echo photon counts is s counts per pulse (cpp), the noise rate is r_{noi} cps. The total noise consists of the dark count of the detector, back-scattering from the optical lens, atmospheric back-scattering, and sky background noise. Among them, the noises from the back-scattering from optics and atmosphere can be filtered out through the range gate. The effective detection probability in a range gate can be described as [40]:

$$P_D = e^{-W} \cdot (1 - e^{-s-n}) \cdot \eta, \tag{3}$$

where $W = r_{\text{noi}} \cdot \left(\gamma \cdot t_{\text{gate}} - t_{\text{echo}}\right)$ is the number of noise before effective return echo within a range gate, γ is the position of the effective return echo in the range gate, generally taking 0.5, t_{gate} is duration of range gate, t_{echo} is the effective echoes distribution width, we take 1 ns here, and $n = r_{\text{noi}} \cdot t_{\text{echo}}$ is the number of noise within the effective echo range.

Each pixel of a $M \times M$ SNSPD/APD array works independently during the detection. Assuming that the arrival time of photons to the arrays are uniformly distributed, the number of noise and effective photons reaching each SNSPD are W/M^2 and $(s + n)/M^2$ in one range gate, separately. Once detected a photon, there is a recovery time till another detection, the duration time called dead time t_{dead}. Only if there is no noise to be alarmed during $t - t_{\text{dead}}$ to the time effective photon arrives t will we make effective measurements. The probability of an effective echo photon can be described as follows:

$$P_{\text{SNSPD}} = 1 - (1 - P_D)^{M^2}. \tag{4}$$

The DCR of APD is 28 kHz [33], and the duration of range gate is 100 ns [32]. This corresponds to 15 m in one-way range, which means a more accurate range prediction for the space target. While the DCR of SNSPD is 100 Hz, the duration of the range gate is 20 μs because of the charge-discharge. The number of measurements within one range gate of APD is once, while more than one measurement within a range gate can be made by SNSPD, except during its recovery periods. At noise level of 2 MHz [41], the detection efficiency of SNSPD and APD are both 30%, with return rates at 0.1–1 cpp, simulation has been conducted for the detection probability as shown in figures 4 and 5. From the analysis in figure 4, the detection performance of SNSPD is superior to APD. The results in figure 5 show that the detection probability increases with increasing the number of pixels of the detector, which highlights the advantages of the array detector. When the echo rate is below 1 cpp, the detection probabilities of the 2×2, 3×3, and 4×4 SNSPD arrays are basically equivalent.

3. Results

3.1. Measurements of LLR at TianQin station

The first echo from the Apollo 15 retro-reflector on the surface of the lunar had been detected on 8 June 2019. Till the same year of 7 November, the distances between TianQin Station and five retro-reflector arrays had been ranged, which shows the capability of routine LLR at TianQin Station if weather permits. Figures 6 to 10 show the typical scatter of observed-calculated (O-C) residuals from the five retro-reflector arrays. The best return rate is over 1 cps for Apollo 15 and Lunokhod 1.

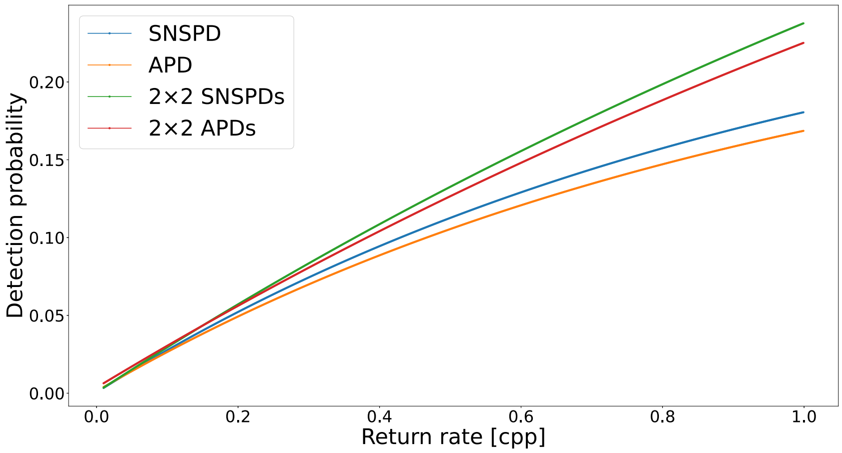

Figure 4. Comparison of detection probability between APD and SNSPD.

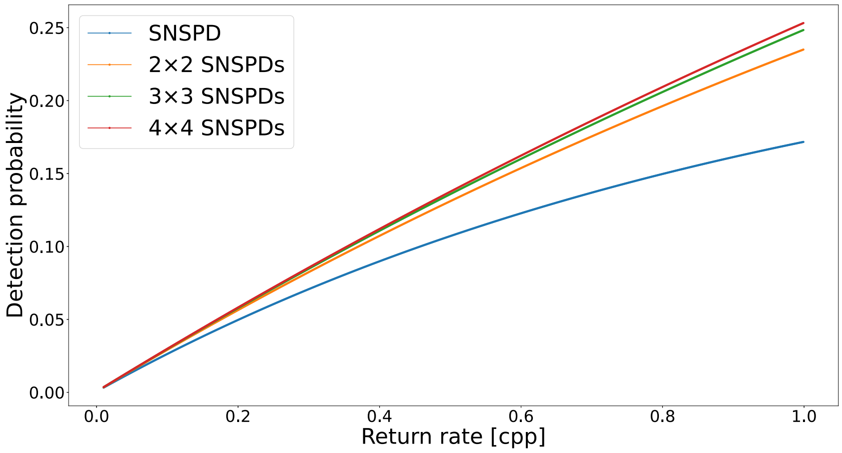

Figure 5. Influence of different number of pixels on detection probability of SNSPD.

From the analysis above, one of the merits of SNSPD lies in high detection efficiency even under the low signal-to-noise ratio (SNR), which means we can get the signal near the full Moon. Figure 11 shows the LLR session on Apollo 15 during Moon phase at 192° (0° and 360° are new Moon, 180° is full Moon). Due to the enhancement of background noise, the SNR of detection decreases, but the effective echo signal can still be extracted from noise easily. Further LLR data near the full Moon will be provided from TianQin Station, which is of great significance to the study of Earth–Moon gravitational theories and lunar ephemeris.

3.2. Precision analysis of SLR and LLR

The random error of laser ranging is determined by the laser ranging system and external factors. The system random errors are introduced by the duration of the laser pulse, time jitter of the detectors (emitting and receiving detectors), GPS clock, event timer, and fiducial signal. The external factors include atmospheric turbulence [42] and retro-reflector array [26, 43].

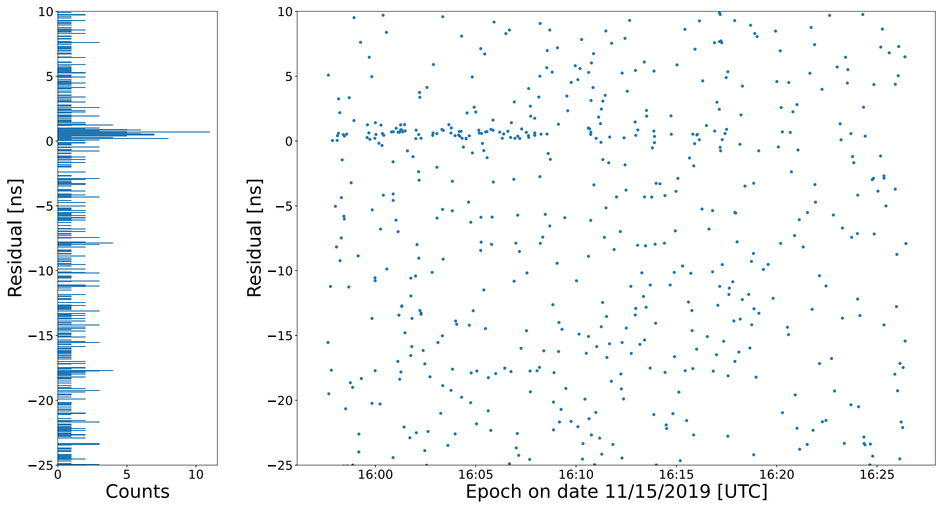

Figure 6. Example of a ranging session on the Apollo 11.

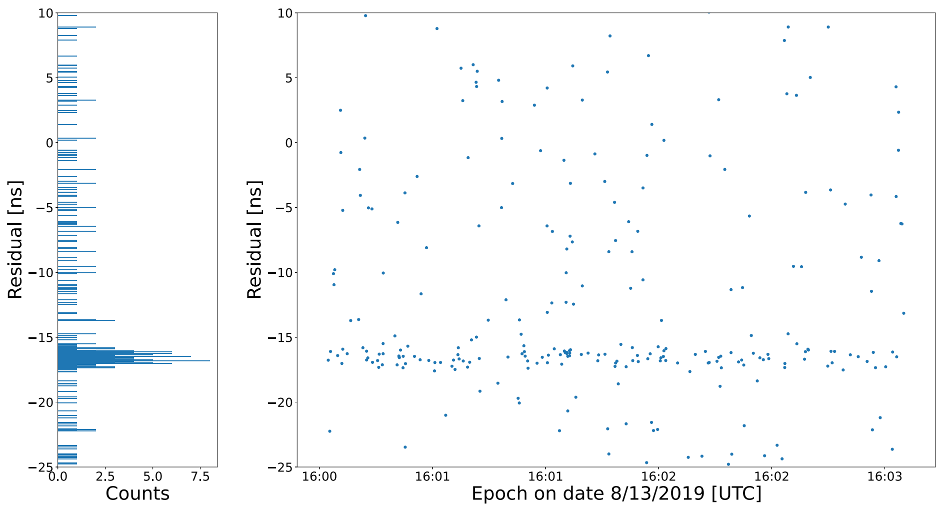

Figure 7. Example of a ranging session on the Apollo 14.

Based on measurements in the laboratory of the timing performance of the individual facilities comprising the system, we derive the random error budget per photon presented in table 3.

3.2.1. Evaluation the SLR accuracy. SLR is an important tool in satellite and space geodesy because it is a technique that can provide independent orbit information. There are some heavy, spherical, passive satellites equipped with corner cubes called geodetic satellites, e.g. Starlette, Stella, LAGEOS, Etalon, GFZ-1, WESTPAC, Larets, LARES, Ajisai, and BLITS which had the potential of centimeter accuracy ranging [44]. There are precision orbit data provided by ILRS [14] in Standard Product 3 (sp3) orbit format. Given a specific time, combined with the

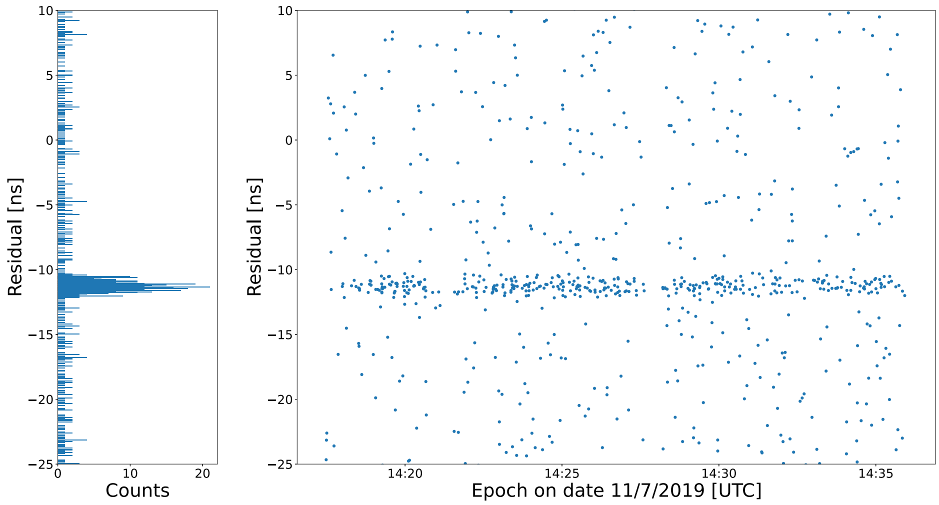

Figure 8. Example of a ranging session on the Apollo 15.

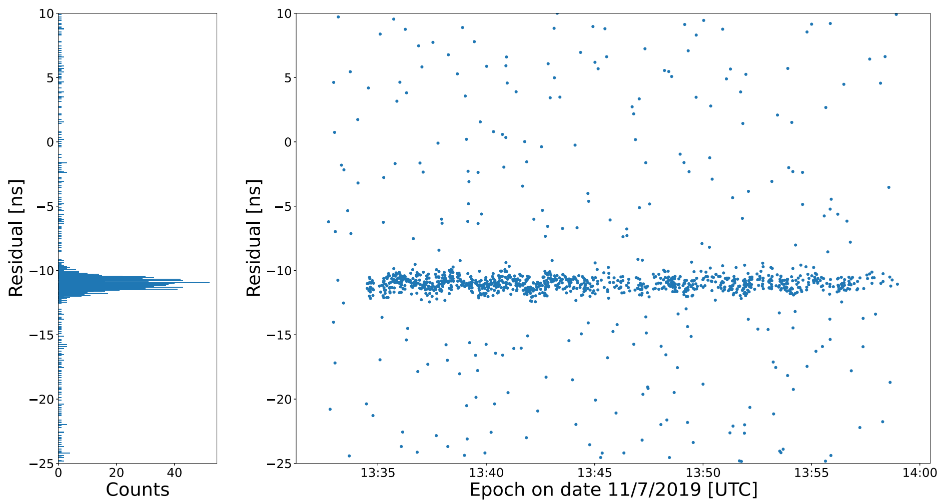

Figure 9. Example of a ranging session on the Lunokhod 1.

sp3 data, it is easy to calculate the single-trip TOF ρ:

$$\rho = \frac{1}{2}\left(\rho_{\text{up}} + \rho_{\text{down}}\right) + \rho_{\text{rel}} + \rho_{\text{atm}} + \rho_{\text{com}} + \epsilon, \tag{5}$$

where ρ_{up} and ρ_{down} are the up-link and down-link pulse travels between the station and target. To acquire precision station coordinates, there exists the Earth tide correction [45]. ρ_{rel} is relativistic gravitational delay of signal propagation [46], ρ_{atm} is the zenith atmospheric delay [47, 48], ρ_{com} is the correction of mass center [49], ϵ is system error bias. The bias can be calculated from measured and precision orbit data [50].

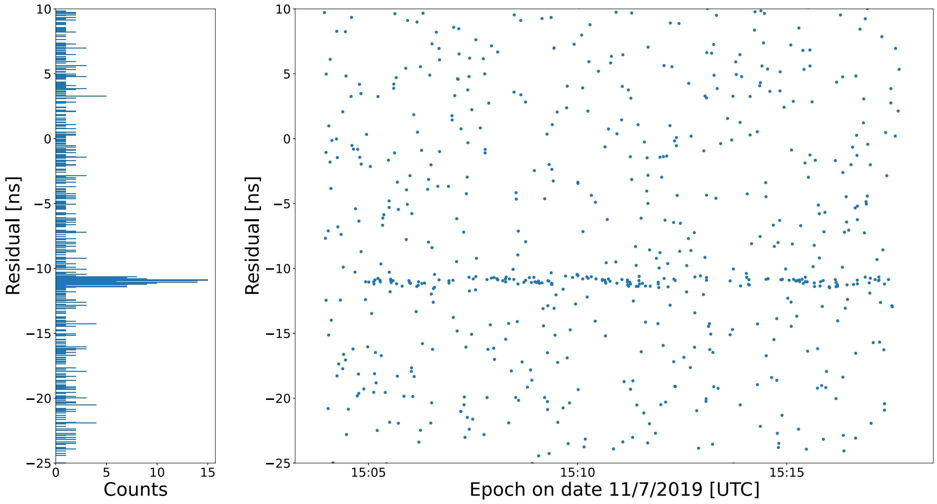

Figure 10. Example of a ranging session on the Lunokhod 2.

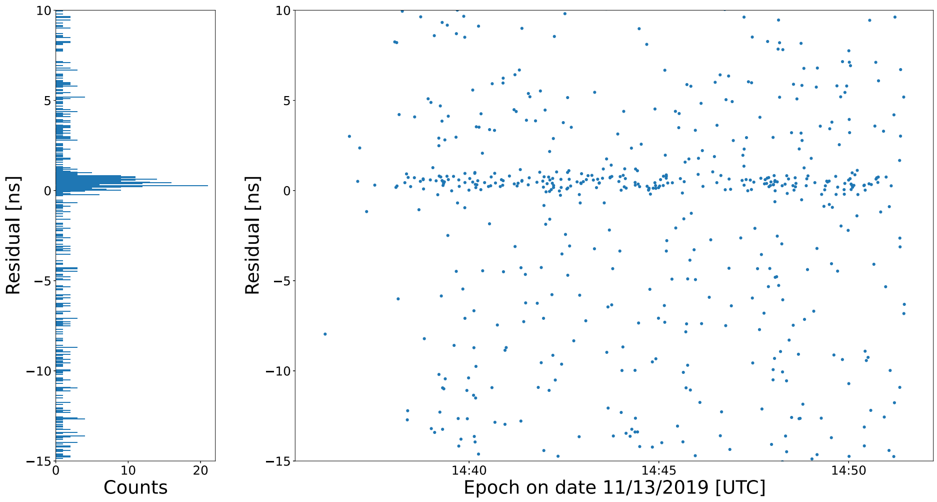

Figure 11. Example of a ranging session on the Apollo 15 near the full Moon.

During a SLR session, the laser up-link and down-link TOF are

$$\tau_{\text{up}} = \frac{1}{c}\left|\boldsymbol{r}\left(t+\tau_{\text{up}}\right) - \boldsymbol{R}(t)\right| + \rho_{\text{rel\_up}} + \rho_{\text{atm\_up}} + \rho_{\text{com\_up}}, \tag{6}$$

$$\begin{aligned}\tau_{\text{down}} = \frac{1}{c}&\left|\boldsymbol{r}\left(t+\tau_{\text{up}}\right) - \boldsymbol{R}\left(t+\tau_{\text{up}}+\tau_{\text{down}}\right)\right| \\ &+ \rho_{\text{rel\_down}} + \rho_{\text{atm\_down}} + \rho_{\text{com\_down}},\end{aligned} \tag{7}$$

where $\boldsymbol{r}\left(t+\tau_{\text{up}}\right)$ is the center coordinates of the satellite on the geocentric inertia system when the pulse arrives the satellite, $\boldsymbol{R}(t)$ and $\boldsymbol{R}\left(t+\tau_{\text{up}}+\tau_{\text{down}}\right)$ are the coordinates of the station on

Table 3. Random error contributes at TianQin Station.

Error sources	Contributed timing electronics error (ps)	Contributed ranging error (mm)
Pulse width	31.6	4.7
Time jitter of (emitting) detector	1.0	0.1
Time jitter of (receiving) detector	39.5	5.9
GPS clock	1.0	0.1
Event timer	0.9	0.1
Calibration of ground target	3.0	0.4
Atmospheric turbulence (seeing: $2''$)	3	0.4
Lunar retro-reflector: Apollo 15	0–240	0–36.0
Total random error	50.8–255	7.6–38.2

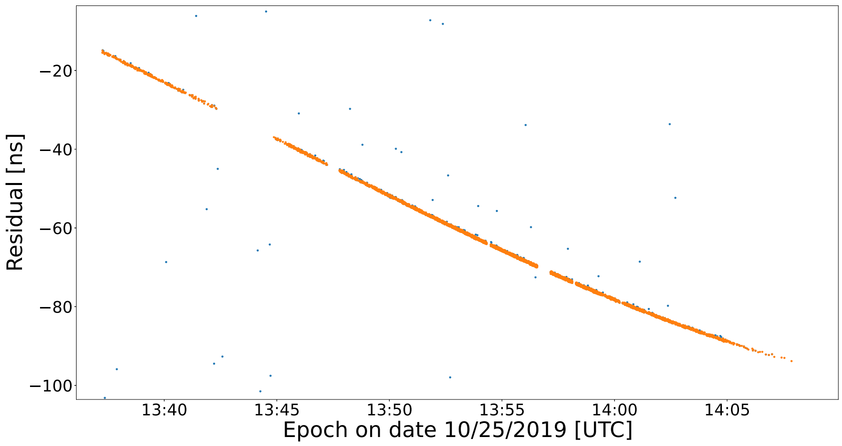

Figure 12. An example of range session on LAGEOS2.

the geocentric inertia system when the pulse is transmitted and the effective return echo is received. The round-trip time of pulses travel between station and target can be calculated through equations (6) and (7). The typical ranging session of SLR carried out by TianQin Station on LAGEOS2 on 25 October 2019 shows in figure 12.

There are system biases at TianQin Station shown in figure 12, which are composed of station eccentricity bias, time bias and fixed bias, etc. The bias and correction will be further analyzed in the follow-up work. Polynomial fitting is performed for the O-C residuals in figure 12. After removing the trend term, the corresponding new residuals can be used for analyzing the random error of TianQin Station. The random error of two-way measurement is 167 ps, corresponding 2.4 cm in one-way range as shown in figure 13.

3.2.2. Checking against models of LLR. The schematic diagram of a pulse travelling between the Earth and the Moon is shown in figure 14, the process involves the motion of the Earth and the lunar. The geocentric coordinates, selenocentric coordinates, and the lunar Euler angles which can be used for transformation between the International Celestial Reference System and principal axis (PA) system can be obtained from ephemeris [51, 52]. Combined with the EarthEOP released by the International Earth rotation and reference systems service

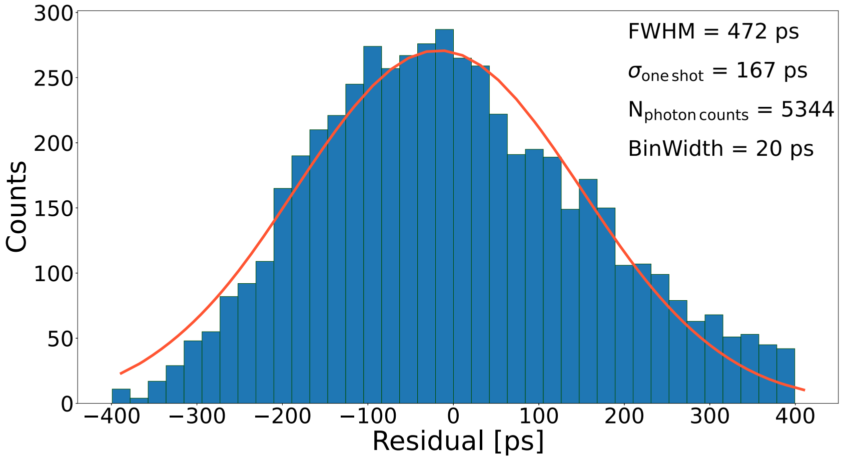

Figure 13. An example of histogram statistics and polyfit on O-C residuals of LAGEOS2.

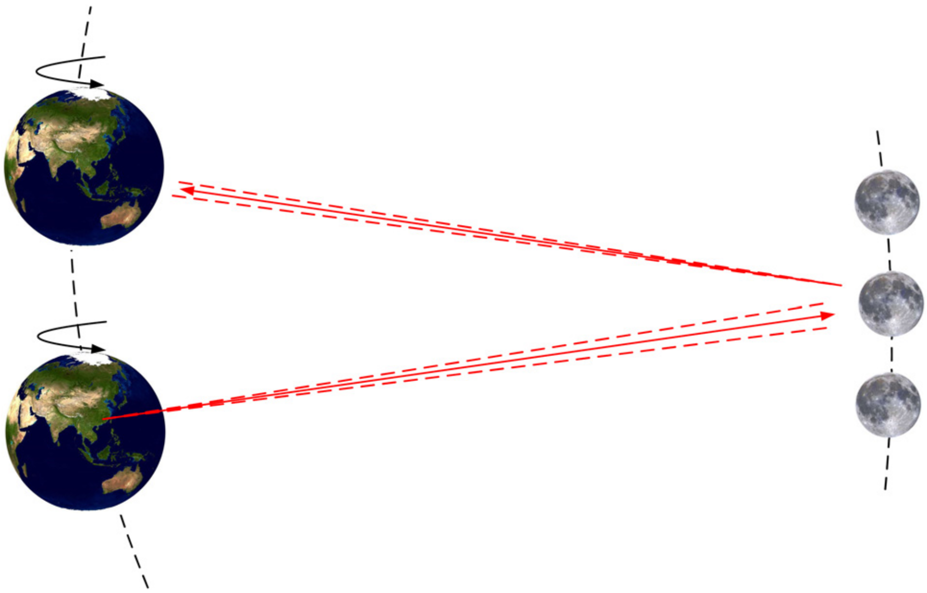

Figure 14. Schematic diagram of LLR.

[53], the round-trip time of the pulse between the station and the lunar retro-reflector can be calculated.

Because all massive Solar System bodies influence the Earth–Moon range, the analysis is most conveniently performed in the Solar System barycenter (SSB) frame. Barycentric celestial reference system (BCRS) and geocentric celestial reference system share the same spatial axes, but different origins, and are associated with the time scale barycentric coordinate time or barycentric coordinate time (TDB) and the time scale geocentric coordinate time. The measured times are transformed into SSB coordinates using the standard time transformation

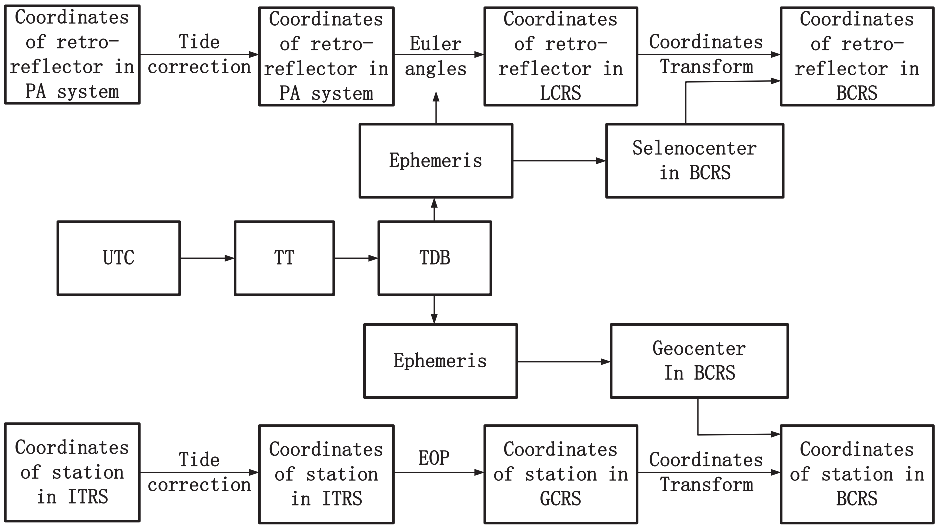

Figure 15. The process to obtain the coordinates of retro-reflector and station in BCRS.

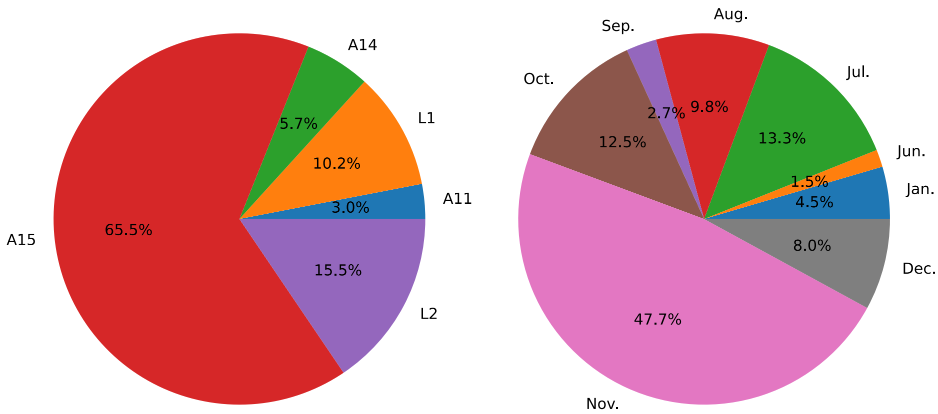

Figure 16. Distribution of NPs on different retro-reflector arrays on the Moon (left). Distribution of NPs on different months over 1.5 years (right).

technique [54]. The LLR up-leg TOF in TDB is [55]

$$t_2 - t_1 = \frac{|\boldsymbol{r}_{\text{BCRS}}(t_2) - \boldsymbol{s}_{\text{BCRS}}(t_1)|}{c} + \Delta t_{\text{rel}}(t_1, t_2) + \Delta t_{\text{atm}}(t_1, t_2), \tag{8}$$

where t_1 is the transmit time through the reference point (the intersection of azimuth and altitude axes of the telescope, also known as the invariant point) of the station and t_2 is the arrival time on the retro-reflector. The LLR down-leg TOF in TDB is

$$t_3 - t_2 = \frac{|\boldsymbol{s}_{\text{BCRS}}(t_3) - \boldsymbol{r}_{\text{BCRS}}(t_2)|}{c} + \Delta t_{\text{rel}}(t_3, t_2) + \Delta t_{\text{atm}}(t_3, t_2), \tag{9}$$

where t_3 is time of receiving at reference point, $\boldsymbol{r}_{\text{BCRS}}$ and $\boldsymbol{s}_{\text{BCRS}}$ are the coordinates of the retro-reflector and the station on BCRS, respectively. Obtaining the $\boldsymbol{r}_{\text{BCRS}}$ and $\boldsymbol{s}_{\text{BCRS}}$ involve

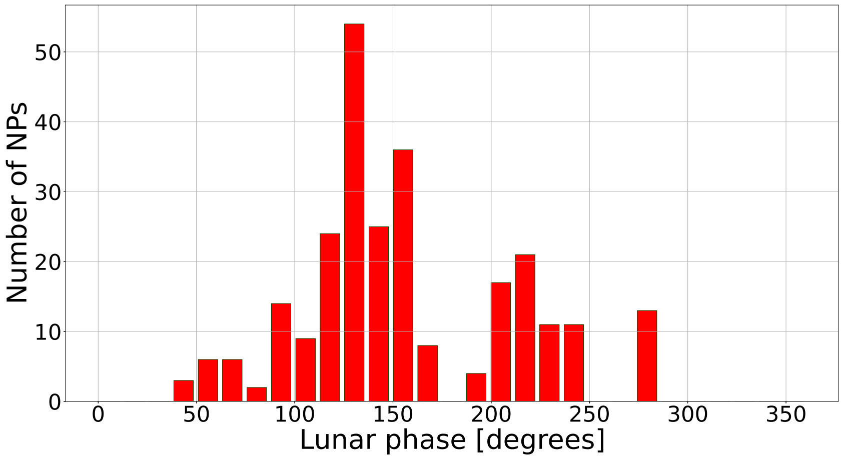

Figure 17. NPs obtained from June 2019 to November 2020 on 5 retro-reflector arrays versus the lunar phase.

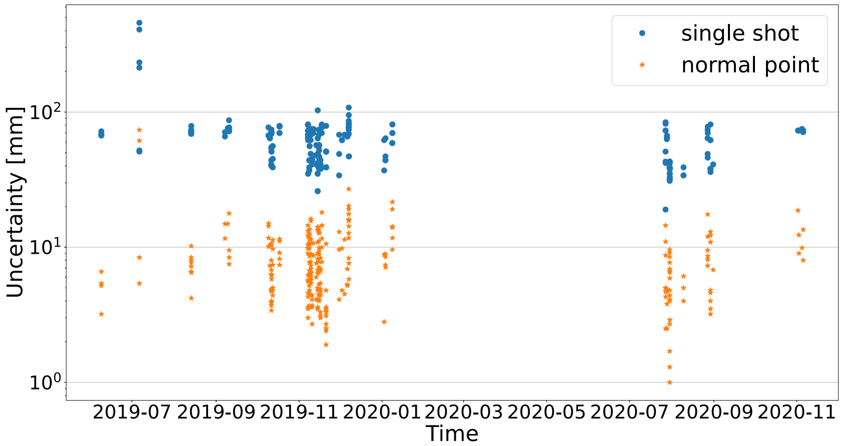

Figure 18. The random error of the 234 NPs.

the coordinate transformation between the International Terrestrial Reference System, the PA system and BCRS. The coordinate acquisition and transformation process is shown in figure 15, and the more specific description can be referred to [55].

3.3. Evaluation of LLR results

A NP is a reduced observation containing the round-trip time of the light pulse at a given time from the spatial reference point of the LLR station on the Earth to the retro-reflector array on the surface of the Moon, computed from many individual measurements, often with the duration of 5–20 min. A NP also contains meteorological parameters and the main parameters of the LLR station. The random error relations between NP and a single shot is

$$\sigma_{\mathrm{NP}} = \left(\frac{\sigma_{\text{single shot}}}{\sqrt{N_{\text{count}}}}\right). \tag{10}$$

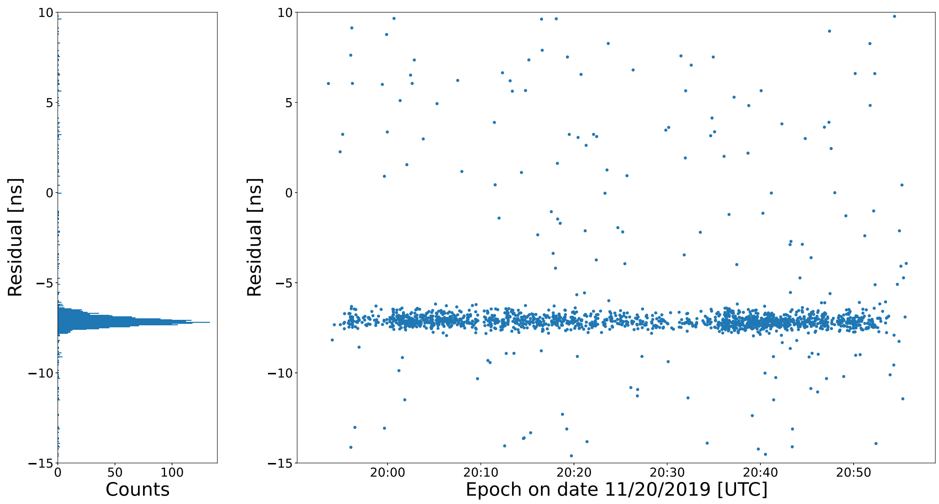

Figure 19. Example of a ranging session on the Apollo 15 reflector panel on 20 November 2019.

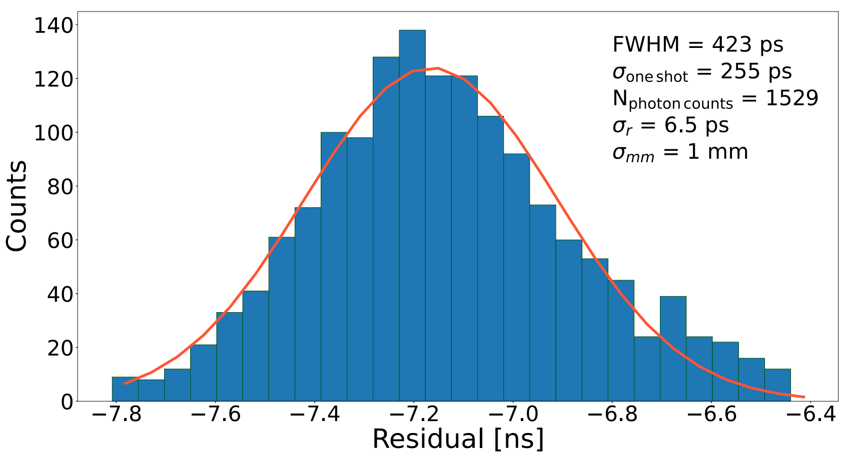

Figure 20. Example of histogram statistics on the Apollo 15 retro-reflector array.

The LLR data acquired by TianQin Station is affected by seasonal weather, the data are mainly distributed in the second half of the year. The main observation target on the surface of the Moon is Apollo 15 due to its largest effective reflection area, as shown in figure 16. The distribution of NPs varies with the phase of the Moon, as shown in figure 17. Routine LLR can also be carried out during the full Moon period.

The precision (i.e. the one-way standard deviation) of all the 234 NPs are illustrated in figure 18. For most NPs, the precision is better than 1 cm, while the corresponding single shot precision is better than 10 cm. The average random error of single shots is about 5.6 cm, the average random error of NP is 7 mm, and the best random errors are 1.5 cm and 1 mm for single shot and NP, respectively. Figures 19 and 20 shows the scatter and histogram of O-C residual of a session on Apollo 15 with a duration of about 1 h. By using the effective echo data to generate a NP, the random error of the NP can reach 1 mm.

4. Conclusion

For precise orbit determination of TianQin satellites, a new laser ranging station with a 1.2 m telescope has been constructed as step 0 of TianQin Project. After months of experiments and having overcome some critical problems, such as the pointing accuracy of the telescope, five retro-reflectors arrays installed on the surface of the lunar have been ranged with the laser ranging system. The successful development of the laser ranging system is conducive to serving for TianQin Project.

LLR observations in green laser have suffered temporal inhomogeneity for many years until the infrared laser has been applied at Grasse. The implementation of 2×2 SNSPD array and pulse with 100 Hz repetition at 1064 nm of TianQin Station provides new opportunities for deep space detection. The effective return rate and ranging accuracy at TianQin Station have met the international advanced level. It will help us to understand the performance of reflectors because of the solar radiation and is of great significance to continuously promote the research and development of Earth–Moon science, such as the libration and inner structure of the lunar. Testing the gravitational theories, such as the equivalence principle, Newton's inverse square law, etc. The station diversity will strengthen significantly the exactitude of the determination of the Moon's trajectory inside our Solar System.

Acknowledgments

The authors thank the support from the National Space Administration, the Ministry of Education, the Guangdong Provincial Government and the Zhuhai Municipal Government, of the People's Republic of China. The authors also thank all members of the TianQin collaboration, project partners, and participants at the workshops for the TianQin science mission, for collaboration and helpful discussions. This work has been jointly funded by National Key R & D Program of China (Grant No. 2020YFC2200200) and Guangdong Major Project of Basic and Applied Basic Research (Grant No. 2019B030302001). This work is based on observation data obtained with the TianQin Station, which is owned and operated by Sun Yat-sen University.

Data availability statement

The data that support the findings of this study are available upon reasonable request from the authors.

ORCID iDs

Caishi Zhang https://orcid.org/0000-0002-9225-6198

References

[1] Luo J *et al* 2016 *Class. Quantum Grav.* **33** 035010
[2] Gong Y, Luo J and Wang B 2021 *Nat. Astron.* **5** 881–9

[3] Ye B, Zhang X, Ding Y and Meng Y 2021 *Phys. Rev.* D **103** 042007
[4] Degnan J J 1993 Millimeter accuracy satellite laser ranging: a review *Contributions of Space Geodesy to Geodynamics: Technology* (Washington, DCAGU) **25** 133–162
[5] Bury G, Sośnica K and Zajdel R 2019 *J. Geod.* **93** 2447–63
[6] Lejba P and Schillak S 2011 *Adv. Space Res.* **47** 654–62
[7] Schillak S, Lejba P and Michałek P 2021 *Sensors* **21** 737
[8] Sośnica K, Jäggi A, Thaller D, Beutler G and Dach R 2014 *J. Geod.* **88** 789–804
[9] Jagoda M and Rutkowska M 2016 *Acta Geod. Geophys.* **51** 493–504
[10] Jagoda M and Rutkowska M 2013 *Adv. Space Res.* **52** 633–8
[11] Sosnica K, Thaller D, Jäggi A, Dach R and Beutler G 2012 *Artif. Satell.* **47** 47
[12] Sośnica K 2015 *Acta Geophys.* **63** 1181–203
[13] Rutkowska M and Jagoda M 2015 *Artif. Satell.* **50** 127
[14] Pearlman M R, Noll C E, Pavlis E C, Lemoine F G, Combrink L, Degnan J J, Kirchner G and Schreiber U 2019 *J. Geod.* **93** 2161–80
[15] Dickey J O *et al* 1994 *Science* **265** 482–90
[16] Murphy T W Jr, Adelberger E G, Battat J B R, Hoyle C D, Johnson N H, McMillan R J, Michelsen E L, Stubbs C W and Swanson H E 2011 *Icarus* **211** 1103–8
[17] Li Y *et al* 2019 *Chin. J. Lasers* **46** 0104004
[18] Williams J G, Turyshev S G and Boggs D H 2009 *Int. J. Mod. Phys.* D **18** 1129–75
[19] Muller J, Hofmann F and Biskupek L 2012 *Class. Quantum Grav.* **29** 184006
[20] Zhang M Y, Muller J and Biskupek L 2020 *Celestial Mech. Dyn. Astron.* **132** 1–15
[21] Nordtvedt K 2001 *Class. Quantum Grav.* **18** L133–7
[22] Müller J and Biskupek L 2007 *Class. Quantum Grav.* **24** 4533–8
[23] Hofmann F, Müller J and Biskupek L 2010 *Astron. Astrophys.* **522** L5
[24] Müller J *et al* 2019 *J. Geod.* **93** 2195–210
[25] Pavlov D 2020 *J. Geod.* **94** 1–14
[26] Battat J B R *et al* 2009 *Publ. Astron. Soc. Pac.* **121** 29
[27] Murphy T W Jr, Adelberger E G, Battat J B R, Hoyle C D, McMillan R J, Michelsen E L, Samad R L, Stubbs C W and Swanson H E 2010 *Icarus* **208** 31–5
[28] Currie D, Dell'Agnello S and Delle Monache G 2011 *Acta Astronaut.* **68** 667–80
[29] Turyshev S G, Williams J G, Folkner W M, Gutt G M, Baran R T, Hein R C, Somawardhana R P, Lipa J A and Wang S 2013 *Exp. Astron.* **36** 105–35
[30] He Y, Liu Q, He J-J, Li M, Duan H-Z, Yeh H-C and Luo J 2018 *Chin. Phys.* B **27** 100701
[31] He Y, Liu Q, Duan H-Z, He J-J, Jiang Y-Z and Yeh H-C 2018 *Res. Astron. Astrophys.* **18** 136
[32] Murphy T W Jr *et al* 2008 *Publ. Astron. Soc. Pac.* **120** 20
[33] Courde C *et al* 2017 *Astron. Astrophys.* **602** A90
[34] Fried D L 1966 *J. Opt. Soc. Am.* **56** 1372–9
[35] Gudimetla V S R and Kavaya M J 1999 *Appl. Opt.* **38** 6374–82
[36] Zheng X *et al* 2021 *Adv. Photon.* **3** 055002
[37] Warburton R E, McCarthy A, Wallace A M, Hernandez-Marin S, Hadfield R H, Nam S W and Buller G S 2007 *Opt. Lett.* **32** 2266–8
[38] Xue L *et al* 2016 *Opt. Lett.* **41** 3848–51
[39] Tang R, Li Z, Li Y, Pi X, Su X, Li R, Zhang H, Zhai D and Fu H 2018 *Opt. Lett.* **43** 5488–91
[40] Li X *et al* 2016 *Acta Opt. Sin.* **36** 0304001
[41] Samain E *et al* 1998 *Astron. Astrophys. Suppl. Ser.* **130** 235–44
[42] Kral L, Prochazka I and Hamal K 2005 *Opt. Lett.* **30** 1767–9
[43] Murphy T W 2013 *Rep. Prog. Phys.* **76** 076901
[44] Pearlman M *et al* 2019 *J. Geod.* **93** 2181–94
[45] Petit G and Luzum B 2010 *IERS Conventions (2010).* Bureau International des Poids et Mesures Sevres (France)
[46] Shapiro I I 1964 *Phys. Rev. Lett.* **13** 789
[47] Mendes V B, Prates G, Pavlis E C, Pavlis D E and Langley R B 2002 *Geophys. Res. Lett.* **29** 53
[48] Mendes V and Pavlis E C 2004 *Geophys. Res. Lett.* **31** 14
[49] Otsubo T and Appleby G M 2003 *J. Geophys. Res.* **108** B4
[50] Guo J, Wang Y, Shen Y, Liu X, Sun Y and Kong Q 2018 *Earth Planets Space* **70** 1–11
[51] Viswanathan V, Fienga A, Minazzoli O, Bernus L, Laskar J and Gastineau M 2018 *Mon. Not. R. Astron. Soc.* **476** 1877–88
[52] Park R S, Folkner W M, Williams J G and Boggs D H 2021 *Astron. J.* **161** 105

[53] Bizouard C, Lambert S, Gattano C, Becker O and Richard J-Y 2019 *J. Geod.* **93** 621–33
[54] Viswanathan V 2017 Improving the dynamical model of the Moon using lunar laser ranging (LLR) and spacecraft data *PhD Thesis* Paris Sciences et Lettres (ComUE)
[55] Pavlov D A, Williams J G and Suvorkin V V 2016 *Celestial Mech. Dyn. Astron.* **126** 1–28